Journal of Applied Mechanics and Technical Physics, Vol. 44, No. 6, pp. 790–795, 2003

RANDOM OSCILLATIONS OF AN ANTIPHASE-EXCITED AEROELASTIC SYSTEM WITH SYNCHRONIZATION

A. L. Tukmakov

UDC 533.6.013.42

We examine synchronization of the oscillatory motion of thin elastic cylindrical plates forming the walls of a channel filled by a gas. The gas motion in the channel is described by a system of Navier–Stokes equations solved by the MacCormack method of second-order accuracy. The motion of the channel walls is described by a system of dynamic, geometrically nonlinear equations of the thin-shell theory; this system is solved by the finite difference method. Kinematic and dynamic contact conditions are set at the interface between the media. By means of a numerical experiment, possible scenarios of the transition of the aeroelastic system to in-phase oscillations were identified, and the regime of random oscillations in the system with synchronization under antiphase external excitation was found.

Key words: *channel with elastic walls, oscillation characteristics, numerical computations.*

The interaction between the elements of a spatially coupled aeroelastic system can give rise to synchronous dynamic regimes [1–3]. If the elements of a dynamic system exhibiting a tendency to synchronization experience antiphase external excitation, then the system dynamics can be irregular. In the present work, we simulate dynamic processes leading to synchronization of the oscillation phase of thin elastic plates forming parts of the upper and lower walls of a plane channel filled by air, investigate possible scenarios of synchronization, and consider the dynamics of the interacting media.

1. Model and System of Equations. We consider a plane channel filled by air with the upper and lower walls being elastic within the interval $-l \leqslant x \leqslant l$ and rigid outside this interval (Fig. 1). Under asymmetric excitation of the elastic walls of the channel by single external pressure pulses, their oscillations with different amplitudes and phases are first observed. With time, synchronization of the dynamics of the aeroelastic system is possible due to the mutual effect of the walls, exerted through the gas medium.

To describe the motion of the gas in the channel, we used the Navier–Stokes equations for an incompressible heat-conducting gas [4] in Cartesian coordinates:

$$\boldsymbol{q}_t + \boldsymbol{F}_x + \boldsymbol{G}_y = 0. \tag{1}$$

Here

$$\boldsymbol{q} = \begin{bmatrix} \rho \\ \rho u \\ \rho v \\ e \end{bmatrix}, \quad \boldsymbol{F} = \begin{bmatrix} \rho u \\ \rho u^2 + p - \tau_{xx} \\ \rho uv - \tau_{xy} \\ (e + p - \tau_{xx})u - \tau_{xy}v + Q_x \end{bmatrix}, \quad \boldsymbol{G} = \begin{bmatrix} \rho v \\ \rho uv - \tau_{xy} \\ \rho v^2 + p - \tau_{yy} \\ (e + p - \tau_{yy})v - \tau_{xy}u + Q_y \end{bmatrix},$$

$$Q_x = -k\,\frac{\partial T}{\partial x}, \quad Q_y = -k\,\frac{\partial T}{\partial y}, \quad p = (\gamma - 1)(e - 0.5\rho(u^2 + v^2)),$$

$$\tau_{xx} = \mu\Big(2\,\frac{\partial u}{\partial x} - \frac{2}{3}\,D\Big), \quad \tau_{yy} = \mu\Big(2\,\frac{\partial v}{\partial y} - \frac{2}{3}\,D\Big), \quad \tau_{xy} = \mu\Big(\frac{\partial u}{\partial y} + \frac{\partial v}{\partial x}\Big), \quad D = \frac{\partial u}{\partial x} + \frac{\partial v}{\partial y},$$

u and v are the velocity components, ρ is the density, e is the total energy, p is the pressure, k is the thermal conductivity, γ is the ratio of specific heats, and μ is the viscosity.

Institute of Mechanics and Mechanical Engineering, Kazan' Scientific Center, Russian Academy of Sciences, Kazan' 420111. Translated from Prikladnaya Mekhanika i Tekhnicheskaya Fizika, Vol. 44, No. 6, pp. 49–55, November–December, 2003. Original article submitted April 8, 2003.

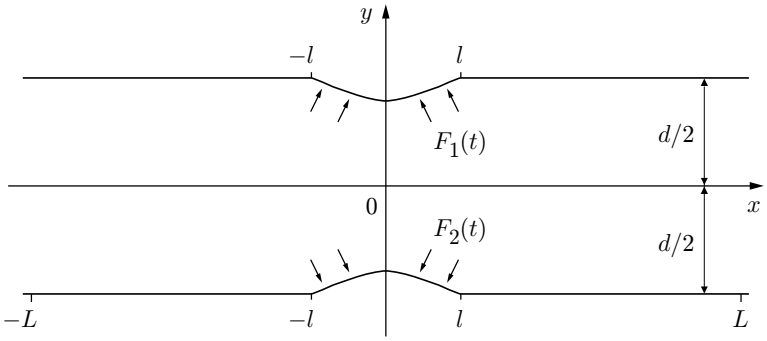

Fig. 1. Schematic of the channel.

In the domain with varied boundaries, system (1) was written in time-dependent generic coordinates [5] and was solved by the explicit MacCormack method of second-order accuracy [4]. The transition to the next time layer was performed through the predictor and corrector steps:

$$\boldsymbol{q}^0_{j,k} = \boldsymbol{q}^n_{j,k} - \frac{\Delta t}{\Delta \xi}\,(\boldsymbol{F}^n_{j+1,k} - \boldsymbol{F}^n_{j,k}) - \frac{\Delta t}{\Delta \eta}\,(\boldsymbol{G}^n_{j,k+1} - \boldsymbol{G}^n_{j,k}),$$

$$\boldsymbol{q}^{n+1}_{j,k} = \frac{1}{2}\,(\boldsymbol{q}^n_{j,k} + \boldsymbol{q}^0_{j,k}) - \frac{1}{2}\,\frac{\Delta t}{\Delta \xi}\,(\boldsymbol{F}^0_{j,k} - \boldsymbol{F}^0_{j-1,k}) - \frac{1}{2}\,\frac{\Delta t}{\Delta \eta}(\boldsymbol{G}^0_{j,k} - \boldsymbol{G}^0_{j,k-1}).$$

At the predictor and corrector steps, the derivatives with respect to ξ in the quantities $\boldsymbol{F}^n_{j+1,k}$ and $\boldsymbol{F}^n_{j,k}$ were replaced by the first-order left and right differences, respectively; the derivatives with respect to η were replaced by second-order central differences. The derivatives with respect to η in the quantities $\boldsymbol{G}^n_{j,k+1}$ and $\boldsymbol{G}^n_{j,k}$ were approximated by the first-order left differences, and the derivatives with respect to ξ were approximated by the central differences. The x step of the finite-difference grid in the physical domain (x, y) was constant. Along the y-axis, the grid contained a fixed number of cells whose size was uniform in each section of the channel. The region (ξ, η) was a unit square with uniform partition along both axes.

To describe the motion of the elastic sectors of the walls, we used a system of dynamic, geometrically nonlinear equations of the theory of thin shells, obtained on the basis of the Kirchhoff–Lové hypothesis [6]:

$$\begin{gathered}\frac{1}{T^2}\,\frac{\partial^2 V}{\partial t^2} - (1+\varepsilon)\,\frac{\partial^2 V}{\partial \alpha^2} - F_1(V,W) = Z_\tau,\\ \frac{1}{T^2}\,\frac{\partial^2 W}{\partial t^2} + \gamma\,\frac{\partial W}{\partial t} + \varepsilon\,\frac{\partial^4 W}{\partial \alpha^4} + W - F_2(V,W) = Z_n;\end{gathered} \tag{2}$$

$$\begin{aligned}F_1 = {}& -\frac{\partial W}{\partial \alpha} + \Big(\frac{\partial V}{\partial \alpha} - W\Big)\Big(\frac{\partial^2 V}{\partial \alpha^2} - \frac{\partial W}{\partial \alpha}\Big) + \Big(\frac{\partial W}{\partial \alpha} + V\Big)\Big(\frac{\partial^2 W}{\partial \alpha^2} + \frac{\partial V}{\partial \alpha}\Big)\\ & + \varepsilon\Big(\Big(\frac{\partial W}{\partial \alpha} + V\Big)\Big(\frac{\partial^2 W}{\partial \alpha^2} - \frac{\partial^3 V}{\partial \alpha^3}\Big) + \frac{\partial^3 W}{\partial \alpha^3} + \Big(\frac{\partial V}{\partial \alpha} - W\Big)\Big(\frac{\partial^3 W}{\partial \alpha^3} + \frac{\partial^2 V}{\partial \alpha^2}\Big)\Big)\\ & + \varepsilon\Big(\Big(\frac{\partial^2 W}{\partial \alpha^2} + V\Big)\Big(\frac{\partial^2 W}{\partial \alpha^2} - \frac{\partial^3 V}{\partial \alpha^3}\Big) + \Big(1 + \frac{\partial V}{\partial \alpha} - W\Big)\Big(\frac{\partial^3 W}{\partial \alpha^3} + \frac{\partial^2 V}{\partial \alpha^2}\Big)\Big)\\ & \times \Big(\Big(\frac{\partial W}{\partial \alpha} + V\Big)\Big(\frac{\partial W}{\partial \alpha} - \frac{\partial^2 V}{\partial \alpha^2}\Big) - \Big(1 + \frac{\partial V}{\partial \alpha} - W\Big)\Big(\frac{\partial^2 W}{\partial \alpha^2} + \frac{\partial V}{\partial \alpha}\Big)\Big),\\ F_2 = {}& -\varepsilon\,\frac{\partial^3 V}{\partial \alpha^3} + \frac{\partial V}{\partial \alpha} + \frac{1}{2}\Big(\frac{\partial V}{\partial \alpha} - W\Big)^2 + \frac{1}{2}\Big(\frac{\partial W}{\partial \alpha} + V\Big)^2\\ & + \varepsilon\Big(\Big(\frac{\partial^2 W}{\partial \alpha^2} + \frac{\partial V}{\partial \alpha}\Big)\Big(\frac{\partial^3 V}{\partial \alpha^3} - \frac{\partial^2 W}{\partial \alpha^2}\Big) + \Big(\frac{\partial W}{\partial \alpha} + V\Big)\Big(\frac{\partial^4 V}{\partial \alpha^4} - \frac{\partial^3 W}{\partial \alpha^3}\Big)\\ & - \Big(\frac{\partial^2 V}{\partial \alpha^2} - \frac{\partial W}{\partial \alpha}\Big)\Big(\frac{\partial^3 W}{\partial \alpha^3} + \frac{\partial^2 V}{\partial \alpha^2}\Big) - \Big(\frac{\partial V}{\partial \alpha} - W\Big)\Big(\frac{\partial^4 W}{\partial \alpha^4} + \frac{\partial^3 V}{\partial \alpha^3}\Big)\Big)\end{aligned} \tag{3}$$

$$+\Big(\frac{\partial V}{\partial\alpha}-W+\frac{1}{2}\Big(\frac{\partial V}{\partial\alpha}-W\Big)^2+\frac{1}{2}\Big(\frac{\partial W}{\partial\alpha}+V\Big)^2\Big)$$

$$\times\Big(\Big(\frac{\partial W}{\partial\alpha}+V\Big)\Big(\frac{\partial W}{\partial\alpha}-\frac{\partial^2 V}{\partial\alpha^2}\Big)-\Big(1+\frac{\partial V}{\partial\alpha}-W\Big)\Big(\frac{\partial^2 W}{\partial\alpha^2}+\frac{\partial V}{\partial\alpha}\Big)\Big).$$

Here W and V are the flexure and tangential displacement of fixed (Lagrangian) points of the median surface, normalized to the radius R of the undeformed panel, Z_τ and Z_n are the tangential and normal components of the dynamic load, $T^2=E/(\rho(1-\nu^2))$, $\varepsilon=\delta^2/12$, $\delta=h/R$, h and ρ are the thickness and density of the panel material, E is Young's modulus, and ν is Poisson's ratio. In the equation for flexure, the term $\gamma(\partial W/\partial t)$ allows for structural damping. Flexure is positive toward the center of curvature, and the tangential displacement is positive in the clockwise direction (see Fig. 1). Anchorage conditions are imposed on the longitudinal edges of the plates (at the points $x=\pm l$).

$$W=0,\qquad V=0,\qquad \frac{\partial W}{\partial\alpha}=0\qquad \text{for}\quad \alpha=\alpha_1,\quad \alpha=\alpha_2. \tag{4}$$

Initially, the elastic walls are assumed to be motionless:

$$W=0,\qquad V=0,\qquad \frac{\partial W}{\partial t}=0,\qquad \frac{\partial V}{\partial t}=0\qquad \text{at}\quad t=0,\quad \alpha_1\leqslant\alpha\leqslant\alpha_2. \tag{5}$$

The normal component of the dynamic load contains the rigid and follow-up parts, and the tangential component is zero. The follow-up character is defined by the excess pressure acting on the elastic surface. The rigid component of loading is defined by the external excitation $F(t)$ uniformly distributed over the plate surface; this component is independent of the plate shape:

$$Z_n=F(t)+K(p_0-p),\quad Z_\tau=0,\quad F(t)=F_0t\quad \text{at } t<T_{\text{load}},\qquad F(t)=0\quad \text{for } t\geqslant t_{\text{load}}. \tag{6}$$

Here p and p_0 are the current and undisturbed gas pressures at the times t and $t=0$, $K=p_0R(1-\nu^2)/(Eh)$, and t_{load} is the time of increasing of the external load pulse.

Subject to conditions (3)–(6), system (2) was solved by the finite difference method with the use of second-order implicit difference schemes [7]. In analyzing the solution of the system, we constructed the power spectrum of the signal [1]

$$|\bar X_k|^2=\Big|\frac{1}{\sqrt{n}}\sum_{j=1}^{n}X_j\exp\Big(-i\,\frac{2\pi kj}{n}\Big)\Big|^2,$$

where X_j is the central flexure of the plate at the time $t_j=j\Delta t$, $|\bar X_k|^2$ is the discrete time-dependent component of the power spectrum, and Δt is the time step.

The change in the shape of elastic elements altered the computational domain geometry. The finite-difference grid in the "physical" variables x, y and its mapping onto a motionless finite-difference grid in the variables ξ and η were reconstructed at each time step. The reconstruction parameters ξ_x, ξ_y, η_x, η_y, x_t, y_t, ξ_t, and η_t entering into the system of equations of gas motion, which was written in generic moving coordinates [5], were determined, and the transition to the next time layer was performed using the MacCormack scheme.

Kinematic and dynamic contact conditions were set at the interface between the media. No-slip conditions were imposed on the solid surfaces for gas-velocity components: at points on the plate surface, they were assumed to be equal to the corresponding components of the plate velocity. Nonreflecting boundary conditions were set for the longitudinal component of velocity at the input and output boundaries of the channel [8], and uniform boundary conditions of the second kind were imposed for the transverse component of velocity:

$$u_{J,k}=u_0+\frac{2c_0}{\gamma-1}\Big(\Big(\frac{p_{J-1,k}}{p_0}\Big)^{(\gamma-1)/(2\gamma)}-1\Big),\qquad v_{J,k}=v_{J-1,k},$$

$$u_{1,k}=u_0-\frac{2c_0}{\gamma-1}\Big(\Big(\frac{p_{2,k}}{p_0}\Big)^{(\gamma-1)/(2\gamma)}-1\Big),\qquad v_{1,k}=v_{2,k}.$$

Here u_0, c_0, and p_0 are the initial gas velocity, speed of sound in the gas, and pressure. Uniform boundary conditions of the second kind were set at all boundaries of the computational domain for density, energy, and temperature. The temperature, density, and velocity of the gas were determined in internal nodes at the initial time.

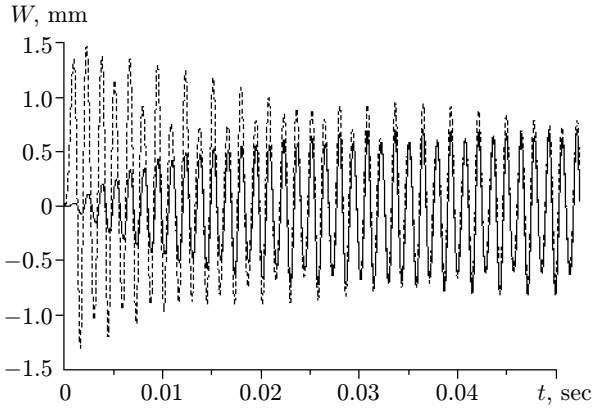

Fig. 2. Synchronization of panel oscillations in the system excited by a single pulse.

The gas-dynamic part of the software package was tested by comparing the results of numerical simulation with available experimental data [9]. The method used to model the dynamics of the elastic element was considered in [7].

The numerical experiment included simulation of aeroelastic oscillations arising under loading of elastic walls of the channel by single triangular pressure pulses whose duration was equal to half of the period of eigenoscillations of the plates at the lower resonant frequency. The calculations for a channel of height $d = 0.15$ m were performed for the following values of elastic plate parameters: thickness $h = 0.001$ m, radius of curvature $R = 1.5$ m, distance between the longitudinal edges of the panel $2l = 0.4$ m, elasticity modulus $E = 10^{11}$ N/m^2, Poisson's ratio $\nu = 0.3$, and density $\rho_n = 4500$ kg/m^3. The number of nodes of the finite-difference grid in solving the elastic problem was $N = 80$. The following characteristics were used for the gas (air) filling the channel: ratio of specific heats $\gamma = 1.4$, initial temperature of the undisturbed gas $T_0 = 290$ K, and initial density $\rho_0 = 1.2$ kg/m^3. The results were obtained on a computational grid with parameters $N_j = 297$ and $N_k = 40$ (N_j and N_K are the numbers of nodes of the finite-difference grid in the longitudinal and transverse directions). The artificial input and output boundaries of the computational domain were located in the cross sections $x = \pm L$. The time step in the computations was $\Delta t = 3 \cdot 10^{-8}$ sec, and the channel length was $2L = 3$ m.

2. Synchronization Scenarios for Aeroelastic Oscillations. If the elastic elements have identical parameters, then the dynamics of the system and the scenarios of its synchronization are determined by characteristics of external exciting pulses $F_1(t)$ and $F_2(t)$ acting on the elastic walls of the channel.

We consider a dynamic process arising if the external load pulse is applied to only one elastic wall: $F_1(t) = At$ for $t < t_{\text{load}}$ and $F_1(t) = 0$ for $t > t_{\text{load}}$; $F_2(t) = 0$. In this case, the oscillations of the second wall arise due to aeroelastic interaction. Figure 2 shows the flexure of the plates in time. The amplitude of oscillations of the plate to which the external pressure pulse was applied decreases with time (the energy of oscillations of this plate is spent on swinging the second plate and irradiating waves in the gas propagating along the channel). The increase in the amplitude of oscillations of the initially motionless plate is accompanied by a decrease in the phase shift. At the end of the first half-period, the phase shift of oscillations of the plates is $\pi/2$, but the phase difference of oscillations decreases with time, and oscillations are synchronized both in terms of amplitude and phase at $t > 0.04$ sec (Fig. 2). The oscillations of both plates are amplitude-modulated with a frequency equal to the difference between the frequency of the first linear resonance of the gas column in the transverse direction ($f_{11} = 1100$ Hz) and the natural frequency of aeroelastic oscillations of the plate ($f = 700$ Hz). Thus, with the external pulse applied only to one elastic wall, synchronization occurs with simultaneous vanishing of the phase and amplitude differences of the oscillating panels. As in the case of oscillating flat plates [3], synchronization of motion is accompanied by a drastic decrease in the amplitude of pressure waves in the case of longitudinal oscillations of the gas in the channel. Prior to synchronization, plate oscillations are accompanied by significant changes in volume of the channel bounded by elastic walls; in-phase displacements of the walls correspond to small changes in the channel volume and to a decrease in the amplitude of pressure oscillations.

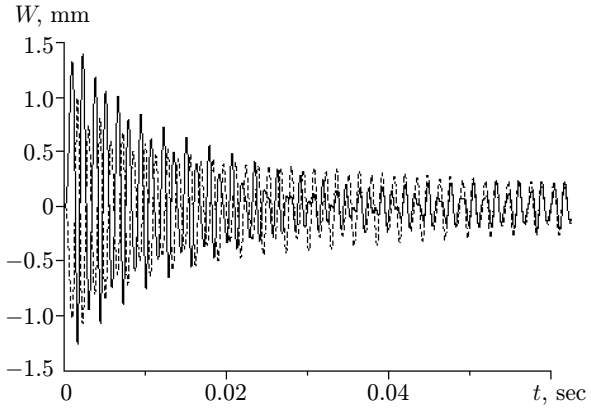

Fig. 3

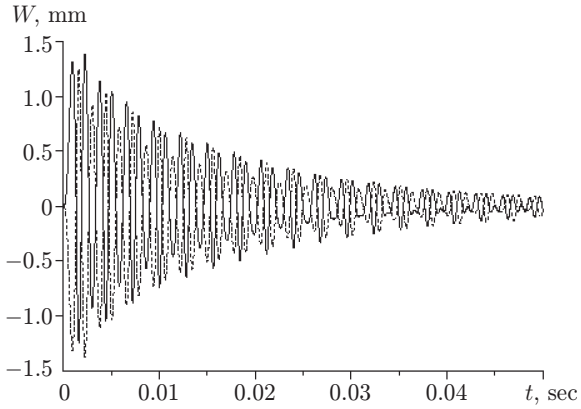

Fig. 4

Fig. 3. Synchronization of panel oscillations under antiphase excitation by pulses of different intensities.

Fig. 4. Antiphase oscillations of the panels in the system excited by pulses of close intensities.

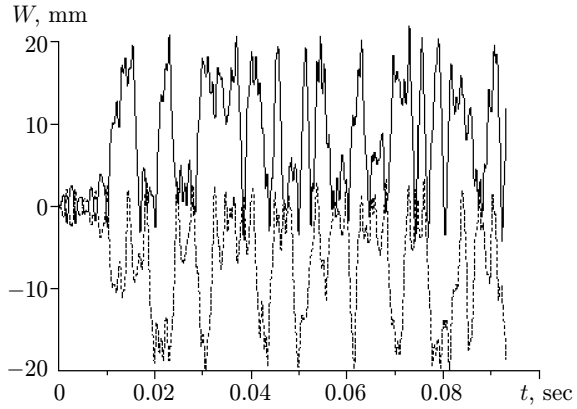

Fig. 5

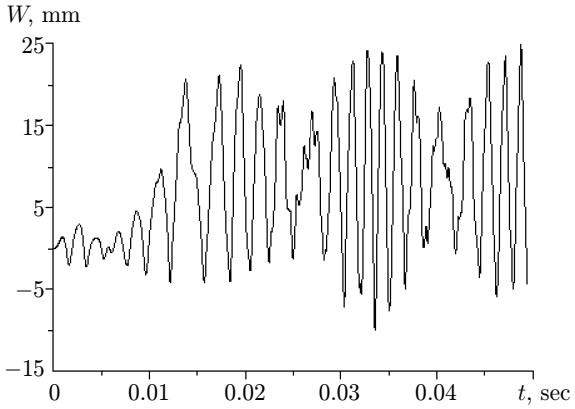

Fig. 6

Fig. 5. Random aeroelastic oscillations of the panels under antiphase excitation.

Fig. 6. Panel oscillations with no allowance for aeroelastic interaction under antiphase excitation.

If the initial excitation of the plates occurs in antiphase with significantly different intensities of external pressure pulses, equalization of oscillation amplitudes of the elastic walls is preceded by phase synchronization owing to extension of the oscillation period of one plate. Figure 3 shows the flexure of the plates as a function of time for $F_1(t) = At$ $(t < t_{\text{load}})$ and $F_1(t) = 0$ $(t > t_{\text{load}})$; $F_2(t) = -0.8F_1(t)$. The process of amplitude synchronization occurs when the in-phase mode is attained (Fig. 3). After synchronization, the amplitude of oscillations of the plates is lower than that in the case of excitation of oscillation of the system by a single pulse.

If the initial excitation of the plates occurs in antiphase with close intensities of external pressure pulses, no in-phase oscillations arise in the system. Figure 4 shows the flexure of the plates as a function of time for $F_1(t) = At$ $(t < t_{\text{load}})$ and $F_1(t) = 0$ $(t > t_{\text{load}})$; $F_2(t) = -0.99F_1(t)$. Intense damping of oscillations of the elastic walls is observed in this regime because the antiphase oscillations damp each other during aeroelastic interaction.

Thus, numerical simulation of aeroelastic interaction allowed us to reveal synchronous dynamics regimes arising in the system under initially asymmetric excitation. For long-duration antiphase aeroelastic oscillations to be excited, symmetric excitation is necessary.

3. Dynamics of the System Under Stationary Antiphase Excitation. We consider nonlinear oscillations that arise in the channel with elastic walls under stationary antiphase excitation. Let both elastic cylindrical panels experience the action of a uniformly distributed harmonic external load: $F_1(t) = F_2(t) = A\sin(2\pi ft)$. Figure 5 shows the time dependence of panel flexure for the critical value of the external-load amplitude A and for

the loading frequency $f = 500$ Hz. The oscillations occur between two equilibrium positions; because of system anisochronism, they are random and their power spectra display long-duration continuous segments [10].

Figure 6 illustrates the oscillations of the elastic panels under the same load, which were calculated disregarding the aeroelastic interaction (the flexure is positive toward the center of curvature of the undeformed panel; the solid and dashed curves coincide). The oscillations are more regular and have a quasiperiodic rather than developed random character (Fig. 6). In this case, the power spectrum of oscillations is almost ruled, with prevalence of the component at the excitation frequency. In addition to large-scale antiphase displacements, the aeroelastic oscillations contain smaller-scale in-phase displacements (Fig. 6). The latter allows us to conclude that the oscillations of the aeroelastic system develop under the action of two factors: antiphase external excitation and tendency of the system to establishment of the synchronous regime, which complicates the dynamics and gives rise to a random regime.

This work was supported by the Tatarstan Republic's Foundation for Research and Development Works (Grant No. 05-5.3-214/2003 (F)) and by the Federal Target Program "Integration" (Grant No. A0012).

REFERENCES

1. H. G. Schuster, *Deterministic Chaos: An Introduction*, Physik-Verlag, Weinheim (1984).
2. I. I. Blekhman, *Synchronization of Dynamic Systems* [in Russian], Nauka, Moscow (1971).
3. A. L. Tukmakov, "Origination of in-phase oscillations of thin plates with aeroelastic interaction," *Appl. Mech. Tech. Phys.*, **44**, No. 1, 64–68 (2003).
4. K. Fletcher, *Computational Techniques for Fluid Dynamics*, Springer-Verlag, Heidelberg (1988).
5. J. L. Steger, "Implicit finite-difference simulation of flow about arbitrary two-dimensional geometries," *AIAA J.*, **16**, No. 7, 679–686 (1978).
6. Kh. M. Mushtari and K. Z. Galimov, *Nonlinear Theory of Elastic Shells* [in Russian] Tatgiz, Kazan' (1957).
7. A. S. Vol'mir, *Shells in Liquid and Gas Flows. Problems of Aeroelasticity* [in Russian], Nauka, Moscow (1976).
8. M. A. Il'gamov, "Nonreflecting conditions on computation-domain boundaries," in: *Dynamics of Shells in Flows*, Workshop Proceedings, Issue 18, Kazan' Phys.-Tech. Inst., Kazan' Branch of the USSR Academy of Sciences (1985), pp. 4–76.
9. A. L. Tukmakov and R. G. Zaripov, "Numerical simulation of subharmonic oscillations of a gas in a closed tube," *Izv. Vyssh. Uchebn. Zaved., Aviats. Tekh.*, No. 1, 64–67 (2001).
10. A. L. Tukmakov, "Nonlinear vibration model of an elastic panel under periodic loading," *J. Appl. Mech. Tech. Phys.*, **41**, No. 1, 171–175 (2000).